Published in final edited form as:
J Am Chem Soc. 2013 August 21; 135(33): 12164–12167. doi:10.1021/ja403542g.

Metal Ion Sensing Using ion Chemical Exchange Saturation Transfer (iCEST)-^{19}F MRI

Amnon Bar-Shir[†,‡], **Assaf A. Gilad**[†,‡,§], **Kannie W.Y. Chan**[†,§], **Guanshu Liu**[†,§], **Peter C.M. van Zijl**[†,§], **Jeff W.M. Bulte**[†,‡,§,#,□,○,*], and **Michael T. McMahon**[†,§,*]

[†]Russell H. Morgan Department of Radiology and Radiological Science, The Johns Hopkins University School of Medicine, Baltimore, Maryland [‡]Cellular Imaging Section and Vascular Biology Program, Institute for Cell Engineering, The Johns Hopkins University School of Medicine, Baltimore, Maryland [#]Department of Biomedical Engineering, The Johns Hopkins University School of Medicine, Baltimore, Maryland [□]Department of Chemical & Biomolecular Engineering, The Johns Hopkins University School of Medicine, Baltimore, Maryland [○]Department of Oncology, The Johns Hopkins University School of Medicine, Baltimore, Maryland [§]F.M. Kirby Research Center for Functional Brain Imaging, Kennedy Krieger Institute, Baltimore, Maryland, USA

Abstract

Although metal ions are involved in a myriad of biological processes, a non-invasive means of detecting free metal ions in a deep tissue remains a formidable challenge. We present an approach for specifically sensing the presence of Ca^{2+} in which the amplification strategy of chemical exchange saturation transfer (CEST) is combined with the broad range in chemical shifts found in ^{19}F NMR to obtain MR images of Ca^{2+}. We exploit the chemical shift change ($\Delta\omega$) of ^{19}F upon binding of Ca^{2+} to the difluoro derivative of [1,2,-bis(o-aminophenoxy) ethane-N,N,-N′,N′, tetra-acetic acid] (5F-BAPTA), by RF labeling at the bound-19F frequency, $\omega_{[Ca\text{-}5F\text{-}BAPTA]}$, and detecting the label transfer to the free-^{19}F frequency, $\omega_{5F\text{-}BAPTA}$. Through the substrate binding kinetics we were able to amplify the signal of Ca^{2+} onto free 5F-BAPTA and thus indirectly detect low Ca^{2+} concentrations with high sensitivity.

Metal ions play a crucial role in a myriad of biological processes, and the ability to monitor real-time changes in metal ion levels is essential for understanding a variety of physiological events. Ca^{2+} has garnered interest due to its involvement in many cellular functions and signaling pathways.[1] Currently, imaging dynamic changes in Ca^{2+} levels is restricted to fluorescence-based methodologies,[2,3] which are limited by low tissue penetration and therefore restrict in vivo Ca^{2+} imaging in deep tissues. Recent advances in the field of molecular magnetic resonance imaging (MRI) has lead to the development of new strategies in the design and synthesis of responsive contrast agents for detecting biologically relevant metal ions. Lanthanide-based complexes[4–7] and modified superparamagnetic iron oxide[8,9] nanoparticles have been developed for Ca^{2+} sensing using MRI. 1,2-bis(o-aminophenoxy) ethane-N,N,N′,N′-tetraacetic acid (BAPTA), was proposed by Tsien[10] as a Ca^{2+} indicator, and later, its difluoro-derivative, 5F-BAPTA, showed large ^{19}F NMR chemical shifts upon chelating divalent cations.[11] The high selectivity of the binding of 5F-BAPTA to Ca^{2+} compared to Mg^{2+}, and the high resolution in the ^{19}F-NMR spectra have been exploited for

Corresponding Authors: Michael T. McMahon: mcmahon@mri.jhu.edu. Jeff W.M. Bulte: jwmbulte@mri.jhu.edu.

Supporting Information file includes experimental methods, discussions and simulations. This material is available free of charge via the Internet at http://pubs.acs.org.

intracellular Ca^{2+} detection in vitro and in vivo.[11–13] However, MR spectroscopy (MRS)-based approaches rely on observation of the ^{19}F resonance of the Ca-5F-BAPTA complex for Ca^{2+} detection resulting in limited spatial resolution due to sensitivity considerations. One alternative, suggested by Kuchel and co-workers,[14] is the possibility to transfer magnetization between bound Ca^{2+} and free 5F-BAPTA during NMR experiments.

Chemical exchange saturation transfer (CEST) is a widely used MRI contrast mechanism in which a dynamic exchange process between radiofrequency labeled protons and bulk water is exploited for contrast enhancement, and has been used for many applications in molecular and cellular MRI.[15–22] We employ a saturation transfer approach that couples ^{19}F- and CEST-MRI for sensing the presence of Ca^{2+} or Mg^{2+} through their substrate binding kinetics, which we have termed ion CEST (iCEST). Using RF labeling at the bound ion [Ca-5F-BAPTA] ^{19}F frequency and detection of label transfer to the free 5F-BAPTA ^{19}F frequency (0 ppm), we are able to amplify the signal of bound Ca^{2+} by a factor of 100. We demonstrate that the resulting Z-spectra display supreme sensitivity to bound Ca^{2+} over other M^{2+} cations.

Figure 1a illustrates the dynamic exchange process between free 5F-BAPTA and its complex with M^{2+}, [M^{2+}-5F-BAPTA]. Upon M^{2+} binding, there is a ^{19}F chemical shift change ($\Delta\omega$) for 5F-BAPTA. If the exchange rate (k_{ex}) between M^{2+}-bound and free 5F-BAPTA is fast on the NMR time scale ($\Delta\omega \ll k_{ex}$), no peak can be resolved as is demonstrated in Figure 1b for Mg^{2+}.

When the k_{ex} is sufficiently slow at the field strength used, a well-defined peak is observed for the [M^{2+}-5F-BAPTA] resonance as is shown for Zn^{2+} (green, $\Delta\omega \gg k_{ex}$) and Ca^{2+} (blue, $\Delta\omega > k_{ex}$). As was previously reported, the observed $\Delta\omega$'s are typical and unique for each ion that is complexed by 5F-BAPTA and ranges from a few ppm in the cases of Ca^{2+}, Zn^{2+}, Ba^{2+}, Sr^{2+}, Cd^{2+}, Pb^{2+} and others to tens of ppm upon binding of Fe^{2+}, Co^{2+} and Ni^{2+}.[11,23] The dissociation constant (K_d) of [M^{2+}-5F-BAPTA] is different for each M^{2+}, and as a result so is the k_{ex} for the process in Figure 1a.[24,38] The Zn^{2+}-5F-BAPTA peak (Figure 1b, green, 4.1 ppm) is sharper than that of Ca^{2+}-5F-BAPTA (Figure 1b, blue, 6.2 ppm), which is correlated with their reported differences in K_d.[23,38] Note that increasing the temperature from 25°C to 37°C (Figure S3) or the addition of high concentrations of fast exchanging ions such as K^+ and Mg^{2+} (Figure S4) lead to an upfield shift of the free 5F-BAPTA resonance at the ^{19}F-NMR spectrum.

The ^{19}F-iCEST properties of 5F-BAPTA in the presence of Ca^{2+} (slow-to-intermediate k_{ex}), Zn^{2+} (very slow k_{ex}) and Mg^{2+} (fast k_{ex}) were determined on a 16.4 T MRI scanner and are summarized in Figure 2 for two different pH values, i.e. 7.2 (Figure 2a–c) and 6.4 (Figure 2d–f). A pronounce saturation transfer contrast was detected in the Ca^{2+} containing solutions (Figure 2a,d) but not in the Zn^{2+} or Mg^{2+} containing solutions (Figure 2b,e or Figure 2c,f, respectively). Importantly, a broad asymmetry is observed at very high fractional Mg^{2+} concentrations (Figure S5b, $\chi_{(5F\text{-}BAPTA/Mg)}$=50:1), which peaks at ~1.8 ppm, a frequency much lower than Ca^{2+} (Figure S5a). For faster ion exchange processes between free 5F-BAPTA and bound M^{2+}-5F-BAPTA, such as the exchange observed for Mg^{2+} (Figure S5b), other CEST imaging methods, such as frequency-labeled exchange (FLEX), may be considered to improve the detection of these ions.[36–37] Interestingly, the $\Delta\omega$ between [Ca-5F-BAPTA] and free 5F-BAPTA was found to be dependent on pH (Figures 2, 3, S1, S2 and S6 and Table S1), but the k_{ex} between [Ca-5F-BAPTA] and 5F-BAPTA was preserved for all examined pH values as determined by Bloch simulations ($190\pm10\ s^{-1}$, Figures 2 and S1).[25]

These results are in a good agreement with a previous report showing that the binding of Ca^{2+} was unaffected at pH 6–8[11] using ^{19}F-MRS. ^{19}F-NMR spectra collected with an internal reference revealed that upon pH change, the frequency of the free 5F-BAPTA shifts but not the frequency of bound M^{2+}-5F-BAPTA (Figure S2). The T_2 values of 5F-BAPTA are also sensitive to pH as can be seen by the broadening in the Z-spectra (Figures 2, S1 and Table S1). The T_2-value changes seem to be dependent on 5F-BAPTA protonation and not k_{ex}-dependent based on the observation that the same Z-spectra line widths were found for solutions containing Mg^{2+} ($\Delta\omega \ll k_{ex}$) and Zn^{2+} ($\Delta\omega \gg k_{ex}$). Figure 3 shows MR images of the samples that have been used in this study, i.e., 10 mM of 5F-BAPTA and 50 μM of M^{2+}. As expected no difference in MR contrast was observed between the samples when using conventional ^{1}H-MRI or ^{19}F-MRI.

However, contrary to the Mg^{2+}- or Zn^{2+}-containing samples, which did not generate iCEST contrast at this concentration, a large iCEST contrast was detected for the Ca^{2+} containing sample when a saturation pulse (B_1=3.6 μT/2000 ms) was applied at the appropriate frequency offset of the [Ca^{2+}-5F-BAPTA] complex, i.e., $\Delta\omega$=6.2 ppm (pH=7.2) and $\Delta\omega$=5.0 ppm (pH=6.4). Figure S6 shows the dependence of $\Delta\omega$ on pH, with $\Delta\omega$ ranging from 2.1 ppm to 6.2 ppm for pH values of 5.6 to 7.2. In addition, iCEST images were acquired for solutions containing mixtures of Ca^{2+} and Mg^{2+} (50 μM Ca^{2+}, 200 μM Mg^{2+}) and Ca^{2+} and Zn^{2+} (50μM Ca^{2+}, 50 μM Zn^{2+}) with 10 mM BAPTA at pH 7.2. The iCEST contrast produced by the Ca^{2+} was still significant (~22%) at $\Delta\omega$=6 ppm for all mixtures (Figure S5). Although high Mg^{2+} concentrations generate iCEST contrast at $\Delta\omega$=1.8 ppm (Figure S5a–b) the larger $\Delta\omega$, smaller k_{ex} of [Ca-5F-BAPTA] and its much higher iCEST contrast makes this approach better for Ca^{2+} sensing (Figure S5b, amplification factor = ×10 for Mg^{2+}, ×100 for Ca^{2+}).

To evaluate the sensitivity of our suggested approach we examined the iCEST contrast at different ratios of Ca^{2+} to 5F-BAPTA (χ_{Ca}, Figures 4a and S7). As clearly shown in Figure S7, Ca^{2+} is easily detected with iCEST MRI at χ_{Ca}=1:1000, where ~11% contrast is observed in the Z-spectrum for this phantom. The same amplification was obtained when 0.5 mM 5F-BAPTA was used to detect 500 nM Ca^{2+} (Figure 4b), showing the potential of iCEST to sense low Ca^{2+} concentrations.

In this study, we show for the first time that spatial information of Ca^{2+} and Mg^{2+} levels can be obtained using amplification of the sensitivity by iCEST with 5F-BAPTA as the ion indicator. One advantage of using 5F-BAPTA as an MRI responsive agent for detecting metal ions over ^{1}H- MRI[26] or ^{129}Xe-MRI[27] based probes is that no attachment of a contrast enhancer is required. The ^{19}F atoms serve on the chelates as the responsive group as well as contrast generators. Hyperpolarized ^{129}Xe-CEST (hyperCEST)[28–30] was the first example of non-^{1}H CEST-MR imaging, although on a gas bubbled into solution instead of solute such as BAPTA. Earlier heteronuclear NMR experiments using magnetization transfer protocols have allowed detection of exchange between two pools of nuclear spins in MRS studies.[14,31,32]

Our study shows the potential of exploiting the iCEST concept using ^{19}F-MRI, as 1:2000 concentration ratios are amplified to 1:20 changes in ^{19}F signal (Figures 4a and S7), i.e., an amplification factor of ~100 for a k_{ex} of 190 s^{-1}. In addition to the advantages of using ^{19}F-MRI, i.e., high γ, 100% natural isotopic abundance, and negligible amount of ^{19}F in soft tissues, [33,34,39] the large range of ^{19}F chemical shifts (about 20 times that of ^{1}H[35]) and the sensitivity of ^{19}F $\Delta\omega$ to the details of the local environment is an ad- vantage for iCEST-based applications. One obstacle of the iCEST approach would be the detectability level of the free ^{19}F-agent. This could be surmounted by collecting high-resolution ^{1}H-MR images, which provide spatial information, and reducing the resolution for iCEST to allow localized

detectability of the ^{19}F-based agent with improved SNR[39] (see SI for detectability discussion). Using paramagnetic ^{1}H CEST probes[7] for detecting Ca^{2+} will allow better spatial resolution and higher SNR compared to iCEST, but also will have a worse sensitivity for detecting low Ca^{2+} concentrations. In the iCEST approach, the signal from low concentration solutes [Ca^{2+}-5F-BAPTA] is amplified through saturation transfer onto the signal of the high concentration free 5F-BAPTA. Since this contrast is dependent on χ_{Ca}, lower concentrations of Ca^{2+} can be detected through simply reducing the free 5F-BAPTA concentrations, when these concentrations are NMR detect-able.[39] This is an advantage of the iCEST approach, since this feature is not available for ^{1}H CEST, which is based on water. Finally, the unique $\Delta\omega$ found for each [M^{2+}-5F-BAPTA] and the diversity of the obtained k_{ex} may be exploited for multi-ion MR imaging approaches in which each ion generates iCEST contrast with an identifiable amplitude and $\Delta\omega$. This concept was shown for different exchangeable protons in ^{1}H-CEST and termed multi-color imaging.[17]

In conclusion, we have developed a new approach for sensing metal ions with spatial information using MRI, in which the amplification strategy of CEST is combined with the $\Delta\omega$ specificity in ^{19}F frequency. The outlined principles can be further extended for designing new iCEST agents to detect other ions.

Supplementary Material

Refer to Web version on PubMed Central for supplementary material.

Acknowledgments

Supported by MSCRFII-0161-00, R01EB012590, R01EB015031, R01EB015032, MSCRFF-0103-00.

References

1. Clapham DE. Cell. 2007; 131:1047. [PubMed: 18083096]
2. Mank M, Griesbeck O. Chem Rev. 2008; 108:1550. [PubMed: 18447377]
3. Tsien RY. Annu Rev Neurosci. 1989; 12:227. [PubMed: 2648950]
4. Angelovski G, Fouskova P, Mamedov I, Canals S, Toth E, Logothetis NK. Chembiochem. 2008; 9:1729. [PubMed: 18604834]
5. Dhingra K, Fouskova P, Angelovski G, Maier ME, Logothetis NK, Toth E. J Biol Inorg Chem. 2008; 13:35. [PubMed: 17874148]
6. Li WH, Fraser SE, Meade TJ. J Am Chem Soc. 1999; 121:1413.
7. Angelovski G, Chauvin T, Pohmann R, Logothetis NK, Toth E. Bioorg Med Chem. 2011; 19:1097. [PubMed: 20691598]
8. Atanasijevic T, Shusteff M, Fam P, Jasanoff A. Proc Natl Acad Sci U S A. 2006; 103:14707. [PubMed: 17003117]
9. Taktak S, Weissleder R, Josephson L. Langmuir. 2008; 24:7596. [PubMed: 18558729]
10. Tsien RY. Biochemistry. 1980; 19:2396. [PubMed: 6770893]
11. Smith GA, Hesketh RT, Metcalfe JC, Feeney J, Morris PG. Proc Natl Acad Sci U S A. 1983; 80:7178. [PubMed: 6417665]
12. Marban E, Kitakaze M, Kusuoka H, Porterfield JK, Yue DT, Chacko VP. Proc Natl Acad Sci U S A. 1987; 84:6005. [PubMed: 3112778]
13. Anderson SA, Song SK, Ackerman JJ, Hotchkiss RS. J Neurochem. 1999; 72:2617. [PubMed: 10349874]
14. Gilboa H, Chapman BE, Kuchel PW. NMR Biomed. 1994; 7:330. [PubMed: 7718434]
15. Bar-Shir A, Liu G, Liang Y, Yadav NN, McMahon MT, Walczak P, Nimmagadda S, Pomper MG, Tallman KA, Greenberg MM, van Zijl PC, Bulte JW, Gilad AA. J Am Chem Soc. 2013; 135:1617. [PubMed: 23289583]

16. Ratnakar SJ, Viswanathan S, Kovacs Z, Jindal AK, Green KN, Sherry AD. J Am Chem Soc. 2012; 134:5798. [PubMed: 22420507]
17. Liu G, Moake M, Har-el YE, Long CM, Chan KW, Cardona A, Jamil M, Walczak P, Gilad AA, Sgouros G, van Zijl PC, Bulte JW, McMahon MT. Magn Reson Med. 2012; 67:1106. [PubMed: 22392814]
18. Longo DL, Busato A, Lanzardo S, Antico F, Aime S. Magn Reson Med. 201210.1002/mrm.24513
19. Li Y, Sheth VR, Liu G, Pagel MD. Contrast Media Mol Imaging. 2011; 6:219. [PubMed: 21861282]
20. Aime S, Carrera C, Delli Castelli D, Geninatti Crich S, Terreno E. Angew Chem Int Ed Engl. 2005; 44:1813. [PubMed: 15723362]
21. Chan KW, Liu G, Song X, Kim H, Yu T, Arifin DR, Gilad AA, Hanes J, Walczak P, van Zijl PC, Bulte JW, McMahon MT. Nat Mat. 2013; 12:268.
22. Liu G, Song X, Chan KWY, McMahon MT. NMR Biomed. 2013; 26:810. [PubMed: 23303716]
23. Kirschenlohr HL, Grace AA, Vandenberg JI, Metcalfe JC, Smith GA. Biochem J. 2000; 346:385. [PubMed: 10677357]
24. Csermely P, Sandor P, Radics L, Somogyi J. Biochem Biophys Res Commun. 1989; 165:838. [PubMed: 2512923]
25. McMahon MT, Gilad AA, Zhou J, Sun PZ, Bulte JW, van Zijl PC. Magn Reson Med. 2006; 55:836. [PubMed: 16506187]
26. Que EL, Chang CJ. Chem Soc Rev. 2010; 39:51. [PubMed: 20023836]
27. Kotera N, Tassali N, Leonce E, Boutin C, Berthault P, Brotin T, Dutasta JP, Delacour L, Traore T, Buisson DA, Taran F, Coudert S, Rousseau B. Angew Chem Int Ed. 2012; 51:4100.
28. Schroder L, Lowery TJ, Hilty C, Wemmer DE, Pines A. Science. 2006; 314:446. [PubMed: 17053143]
29. Seward GK, Bai YB, Khan NS, Dmochowski IJ. Chem Sci. 2011; 2:1103.
30. Kotera N, Tassali N, Leonce E, Boutin C, Berthault P, Brotin T, Dutasta JP, Delacour L, Traore T, Buisson DA, Taran F, Coudert S, Rousseau B. Angew Chem Int Ed. 2012; 51:4100.
31. Kupriyanov VV, Balaban RS, Lyulina NV, Steinschneider A, Saks VA. Biochim Biophys Acta. 1990; 1020:290. [PubMed: 2248962]
32. Alger JR, Shulman RG. Q Rev Biophys. 1984; 17:83. [PubMed: 6091170]
33. Bulte JWM. Nat Biotechnol. 2005; 23:945. [PubMed: 16082363]
34. Ruiz-Cabello J, Barnett BP, Bottomley PA, Bulte JWM. NMR Biomed. 2011; 24:114. [PubMed: 20842758]
35. Brey, WS.; Brey, ML. Encyclopedia of Magn Reson. Chichester: John Wiley & Sons, Ltd; 2007. p. 2063
36. Friedman JI, McMahon MT, Stivers JT, Van Zijl PC. J Am Chem Soc. 2010; 132:1813. [PubMed: 20095603]
37. van Zijl PC, Yadav NN. Magn Reson Med. 2011; 65:927. [PubMed: 21337419]
38. Schanne FA, Dowd TL, Gupta RK, Rosen JF. Environ Health Persp. 1990; 84:99.
39. Ahrens ET, Zhong J. NMR Biomed. 2013; 26:860. [PubMed: 23606473]

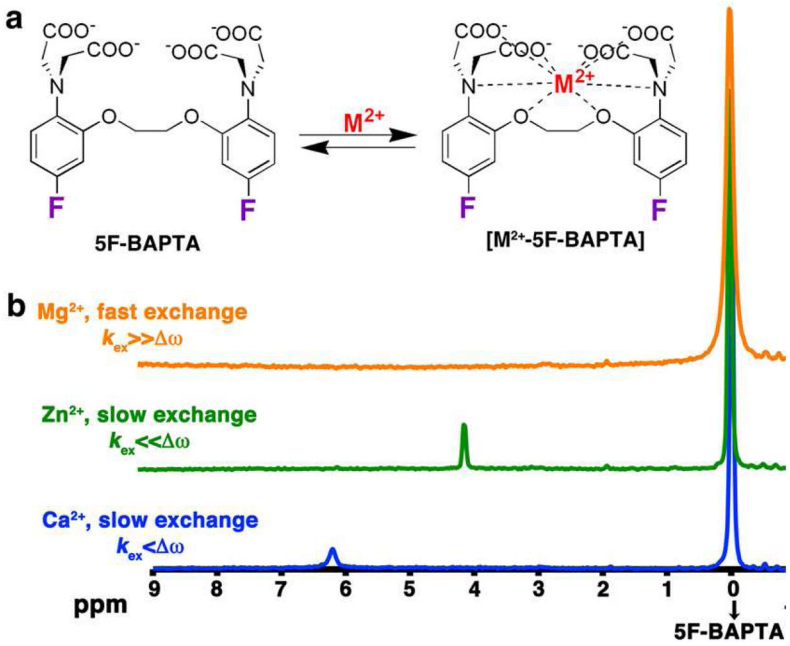

Figure 1.

M^{2+} binding 5F-BAPTA. a) Schematic depiction of the dynamic exchange process between free 5F-BAPTA and bound [M^{2+}-5F-BAPTA]. b) ^{19}F NMR spectra (470 MHz) of 5F-BAPTA in the presence of Mg^{2+} (orange), Zn^{2+} (green), or Ca^{2+} (blue).

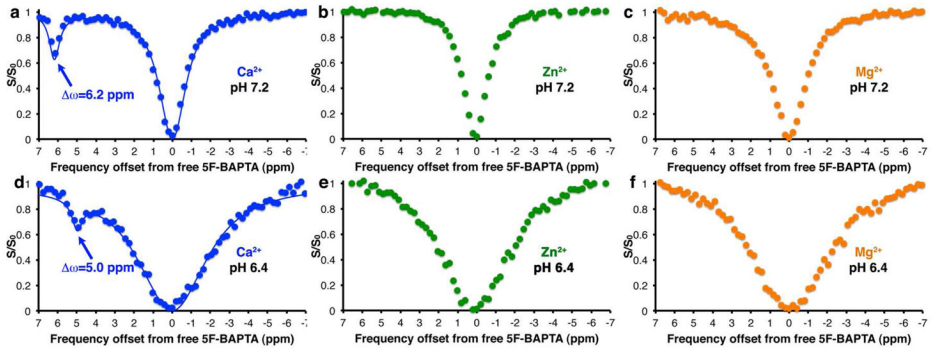

Figure 2.

iCEST characteristics: ^{19}F-iCEST Z-spectra of solutions containing 10 mM of 5F-BAPTA and 50 μM of M^{2+} (M^{2+}: Ca^{2+}, blue; Zn^{2+}, green; or Mg2+, orange) in 40 mM Hepes buffer with the pH of the solutions adjusted to 7.2 (a–c) or 6.4 (d–f). Dots represent the raw experimental data. For Ca^{2+}, lines represent Bloch simulations (two pool model) and arrows point to the frequency of the [Ca^{2+}-5F-BAPTA] complex.

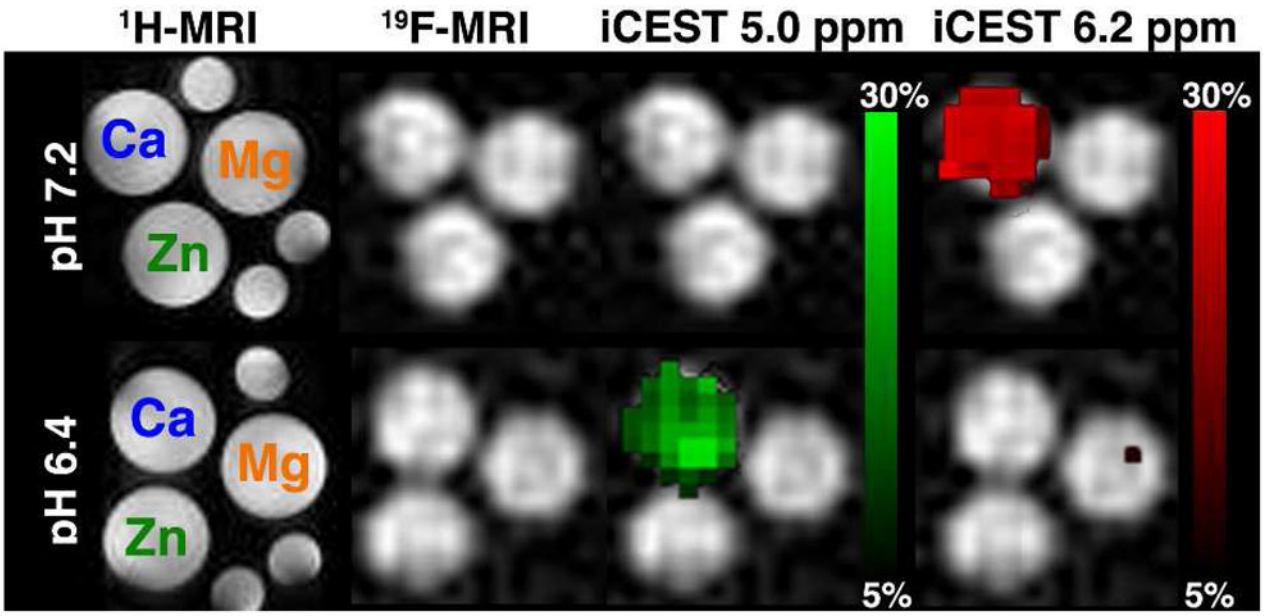

Figure 3.

Imaging Ca^{2+} with iCEST. ^{1}H-MRI, ^{19}F-MRI, and iCEST ($\Delta\omega$=6.2 or 5.0 ppm) of M^{2+} solutions with pH values of 7.2 or 6.4. Each tube contains 10 mM of 5F-BAPTA and 50 μM of M^{2+}. Small water tubes (shown on ^{1}H-MRI) were included to determine the orientation of the samples.

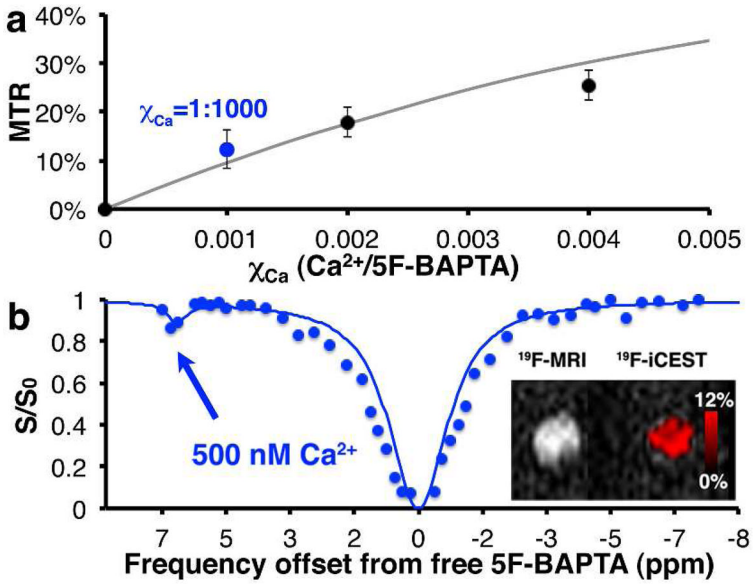

Figure 4.

Ca^{2+} sensing using iCEST. a) χ_{Ca} vs. MTR plot. b) Detection of 500 nM Ca^{2+} in the presence of 0.5 mM of 5F-BAPTA. Inset depicts ^{19}F-MRI of the sample with an overlaid iCEST image. Lines represent Bloch simulations. Error bars represent the inter-voxel standard deviations.